

## Chromium Substituted $\text{LiSn}_2\text{P}_3\text{O}_{12}$ Solid Electrolyte

R. Norhaniza<sup>1</sup>, R.H.Y. Subban<sup>2</sup>, N.S. Mohamed<sup>3,\*</sup>, A.Ahmad<sup>4,\*</sup>

<sup>1</sup> Institute of Graduate Studies, University of Malaya, 50603 Kuala Lumpur, Malaysia.

<sup>2</sup> Faculty of Applied Sciences, Universiti Teknologi MARA, 40450 Selangor, Malaysia

<sup>3</sup> Center for Foundation Studies in Science, University of Malaya, 50603 Kuala Lumpur, Malaysia.

<sup>4</sup> School of Chemical Science and Food Technology, Faculty of Science and Technology, Universiti Kebangsaan Malaysia 43600 Bangi Selangor Malaysia.

\*E-mail: [nsabirin@um.edu.my](mailto:nsabirin@um.edu.my), [azizan@ukm.my](mailto:azizan@ukm.my)

Received: 25 June 2012 / Accepted: 2 September 2012 / Published: 1 October 2012

---

This study was focused on enhancing the conductivity of lithium tin phosphate,  $\text{LiSn}_2\text{P}_3\text{O}_{12}$  by partially substituting  $\text{Sn}^{4+}$  ions with  $\text{Cr}^{3+}$  ions to obtain system with general formula  $\text{Li}_{1+x}\text{Cr}_x\text{Sn}_{2-x}\text{P}_3\text{O}_{12}$ .  $\text{Li}_{1+x}\text{Cr}_x\text{Sn}_{2-x}\text{P}_3\text{O}_{12}$  powders with  $x = 0.2, 0.4, 0.6$  and  $0.8$  were prepared by mechanochemical milling method. X-ray diffraction analysis indicated that all samples consisted of triclinic crystalline  $\text{LiSn}_2\text{P}_3\text{O}_{12}$  structure. Energy Dispersive X-ray analysis suggested that  $\text{Cr}^{3+}$  was successfully substituted into the  $\text{LiSn}_2\text{P}_3\text{O}_{12}$  crystalline structure. Impedance analysis showed an increase in conductivity with increase in  $x$ . The enhancement in bulk conductivity was due to increase in number and polarisability of  $\text{Li}^+$  ions and crystallinity. The increase in grain boundary conductivity was ascribed to enhancement in  $\text{Li}^+$  migration as a result of increase in contact between grains. The conductivity versus the reciprocal of temperature plots showed a sudden change in conductivity at 393 K for the sample with  $x = 0.2$  and 373 K for the sample with  $x = 0.4, 0.6$  and  $0.8$ . This was attributed to a structure transition phenomenon. All samples showed Arrhenian behaviour.

---

**Keywords:** Tin, Conductivity, Nasicon, Arrhenius, Nanomaterial, Solid Electrolyte

### 1. INTRODUCTION

Extensive studies on lithium ion conductor with NASICON (Sodium Superionic Conductor) structure have been done because of their possible application in electrochemical devices [1-4]. NASICON has chemical formula  $\text{LiM}_2\text{P}_3\text{O}_{12}$  ( $M = \text{Ti, Ge, Sn, Zr, Hf, etc.}$ ) with structure built from  $\text{MO}_6$  octahedra and  $\text{PO}_4$  tetrahedra. Their framework is formed by the corner sharing of oxygen of  $\text{PO}_4$  tetrahedra with two  $\text{MO}_6$  octahedra. In this framework there are two probable sites for  $\text{Li}^+$  ions to

occupy i.e.: (i)  $M_1$  sites located between  $MO_6$  octahedral and (ii)  $M_2$  sites, located between the ribbons of  $PO_4$  tetrahedra. This 3D structure possesses channels which are also known as bottlenecks that allow migration of mobile ions. The corner sharing bonding in this framework also allows rotation of the framework; hence modifications like partial substitution may be done to improve its properties [2-4].

In the NASICON family,  $LiSn_2P_3O_{12}$  has received less attention since their pellets were fragile and easily broken making them difficult to handle during characterisation [4-7]. This was due to structure transition (monoclinic to rhombohedral structure) which yielded changes in the lattice volume leading to breakage of the pellet. Several works have been done to overcome this problem such as the use of teflon as a binder [6-7] or the use of germanium (Ge) as an agent for completing the reaction to produce  $LiSn_2P_3O_{12}$  [8]. In our previous study, we have proven that mechanically stable  $LiSn_2P_3O_{12}$  pellets could be obtained by preparing this compound using mechanochemical milling technique without the use of any binding agent [9]. However, the  $LiSn_2P_3O_{12}$  pellets showed low conductivities due chemical composition and ionic mobility.

The present study focussed on enhancing the conductivity of  $LiSn_2P_3O_{12}$  by partially substituting  $Sn^{4+}$  ions with  $Cr^{3+}$  ions. The effects of partial substitution using  $Cr^{3+}$  on conductivity of NASICON structured compounds have been investigated by several researchers [10-13]. According to Zhao et al [14], partial substitution can be easily carried out if the size of the ion is about the same as that of the ion to be substituted. Since the ionic radius of  $Cr^{3+}$  ion is 0.62 Å while that of  $Sn^{4+}$  ion is 0.65 Å, therefore partial substitution of  $Sn^{4+}$  by  $Cr^{3+}$  is expected to be possible. Xu et al reported on conductivity enhancement of about three orders of magnitude for  $Cr^{3+}$  substituted  $LiGe_2P_3O_{12}$  system [10]. Delmas et al [11] reported that the conductivity enhancement in  $Cr^{3+}$  substituted  $NaZrP_3O_{12}$  was due to increase in mobility of ions as reflected by decrease in activation energy. This partial substitutions were done with the objectives of creating Li interstitials to form structures with general formula  $Li_{1+x}Cr_xSn_{2-x}P_3O_{12}$  where  $Sn^{4+} \leftrightarrow Li^+ + Cr^{3+}$  [10-14]. The effects of Cr substitution on the structure and conductivity of  $LiSn_2P_3O_{12}$  are reported in this article.

## 2. EXPERIMENTAL

### 2.1. Materials and Methods

Stoichiometric proportions of  $Li_2O$  (99 % Aldrich),  $Cr_2O_3$ ,  $SnO_2$  (98 % Sigma-Aldrich) and  $NH_4H_2PO_4$  (98 % Sigma-Aldrich) were mixed according to the formula  $Li_{1+x}Cr_xSn_{2-x}P_3O_{12}$  ( $x = 0.2, 0.4, 0.6$  and  $0.8$ ) and heated at 700 °C for two hours. The heating process was required in order to decompose hydrogen phosphate and initiate reaction with carbonate [13,15]. After the heating process, the mixtures were milled for 80 hours using Frisch 7 planetary ball mill. The milled powders were then pelletized to form pellets with diameter of 13 mm and thickness of ~ 1 mm using a hydraulic press at a pressure of 7 ton. The pellets were then sintered at four different temperatures from 700 to 1000 °C for 8 hours. However, it was observed that for different  $x$  values, optimum conductivity was achieved at different sintering temperatures which were at 700, 800, 900 and 1000 °C for  $x = 0.2, 0.4, 0.6$  and  $0.8$  respectively. Therefore, for further analyses, samples were prepared by sintering them at

their optimum sintering temperatures and these samples are labelled as C2, C4, C6 and C8 for  $x = 0.2$ , 0.4, 0.6 and 0.8 respectively.

Structural study was carried out using Bruker D8 Advance X-Ray Diffractometer. Crystallite size,  $D$  was calculated using Scherer equation;

$$D = \frac{k\lambda}{\beta \cos \theta} \quad (1)$$

where  $k$  is the Scherer constant value (0.94),  $\lambda$  is the wavelength of the source (Copper-K,  $\lambda = 1.5406 \text{ \AA}$ ),  $\beta$  is FWHM (in radians) and  $\theta$  is the Bragg angle (in radians). Surface morphology and elemental composition analyses were done using FEI Quanta 200 FESEM equipment in low vacuum condition and accelerating voltage of 20 kV. For these analyses, samples were gold sputtered after ultrasound cleaning. Conductivity studies were carried out using Solartron 1260 impedance analyser. Transference number was determined using Wagner's polarisation method on Solartron 1260 interfaced with SI 1287 Electrochemical Interface. The samples were sandwiched between two carbon electrodes and polarised by applying a potential of 0.5 V.

### 3. RESULTS AND DISCUSSION

#### 3.1. X-ray diffraction (XRD) study

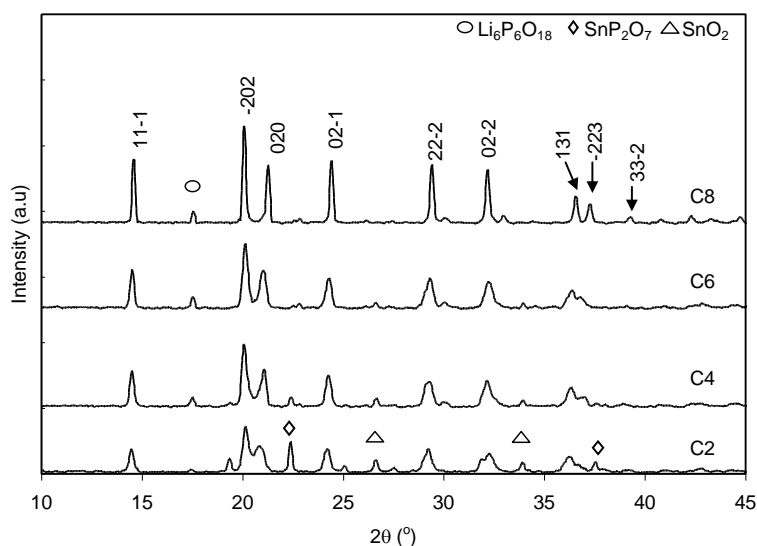


**Figure 1.** X-ray diffraction patterns for C2, C4, C6 and C8

Fig. 1 shows XRD spectra of samples C2, C4, C6 and C8. Presence of crystalline triclinic  $\text{LiSn}_2\text{P}_3\text{O}_{12}$  (labelled with  $hkl$  index in Fig. 1) was detected in all samples. The values of lattice constants of this structure for all samples were similar with those reported by Iglesias which were  $a = 14.680 \text{ \AA}$ ,  $b = 8.413 \text{ \AA}$  and  $c = 8.900 \text{ \AA}$  [16]. Our studies [9] on unsubstituted  $\text{LiSn}_2\text{P}_3\text{O}_{12}$  showed presence of rhombohedral structure with lattice constant values of  $a = 8.650 \text{ \AA}$ ,  $b = 8.650 \text{ \AA}$  and  $c =$

21.487 Å. The change from rhombohedral structure in the unsubstituted  $\text{LiSn}_2\text{P}_3\text{O}_{12}$  to triclinic structure in the chromium substituted samples may be due to the presence of interstitial  $\text{Li}^+$  ions at the mid way sites of  $M_1$  and  $M_2$  [1,3]. The change in structure may also be attributed to the restructuring of the lattice atoms in order to accommodate  $\text{Cr}^{3+}$  ions which were smaller compared to  $\text{Sn}^{4+}$  ions. The adjustment in lattice parameters was due to the expansion of the framework along the  $a$ -axis which caused a rotation of tetrahedral  $\text{PO}_4$  units connecting two parallel columns with a concomitant contraction of the structure along  $c$ -axis [17,18].

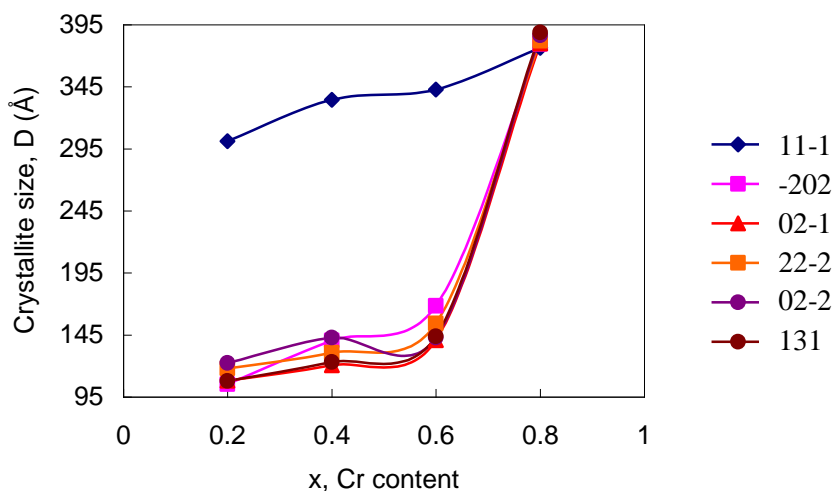


**Figure 2.** Variation of crystallite size with  $x$  (chromium content) at different planes

The peaks of the  $\text{LiSn}_2\text{P}_3\text{O}_{12}$  triclinic crystalline structure were also observed to become narrower with increase in  $\text{Cr}^{3+}$  content showing that Cr substitution controlled the number of nucleation centres resulting in the formation of larger crystallites [19]. Increase in XRD intensity with  $x$  value was due to the growth of  $\text{LiSn}_2\text{P}_3\text{O}_{12}$  structure [10, 20]. In order to determine the crystallite size, Scherrer equation was used and the values of crystallite sizes for  $\text{LiSn}_2\text{P}_3\text{O}_{12}$  are shown in Fig. 2. C8 possessed the largest crystallite size in the range 37 to 38 nm while C2, C4 and C6 possessed crystallites in the range from 11 to 30 nm, 12 to 33 nm and 14 to 34 nm, respectively. This inferred that samples were nanomaterials. Fig. 2 also shows that the crystallite size in C8 was homogeneous while those in other samples were quite heterogeneous. Traces of  $\text{SnP}_2\text{O}_7$  crystalline indicated by the peak at  $2\theta \sim 23^\circ$  was found to be present in all samples. However, the amount of  $\text{SnP}_2\text{O}_7$  decreased with increase in  $x$ . Meanwhile, trace of  $\text{Li}_6\text{P}_6\text{O}_{18}$  was also found to be present in C4, C6 and C8 as indicated by the presence of the peak at  $2\theta \sim 17.5^\circ$ .

### 3.2. Scanning Electron Microscopy (SEM)

Fig. 3 illustrates the SEM micrograph for the cross-sections of C2, C4, C6 and C8. Average grains size in the samples increased with Cr content which were 0.12  $\mu\text{m}$ , 0.45  $\mu\text{m}$ , 0.49  $\mu\text{m}$  and 0.67  $\mu\text{m}$  for C2, C4, C6 and C8 respectively. A notable difference in the grain size was observed in C2.

Decrease in number of large grains was seen in C4. Increase in number of grains with similar size and also contacts between grains were noticed in C6 while C8 exhibited very dense and well-packed structure with fewer pores. Uniform grains that fused together were also observed in this sample.

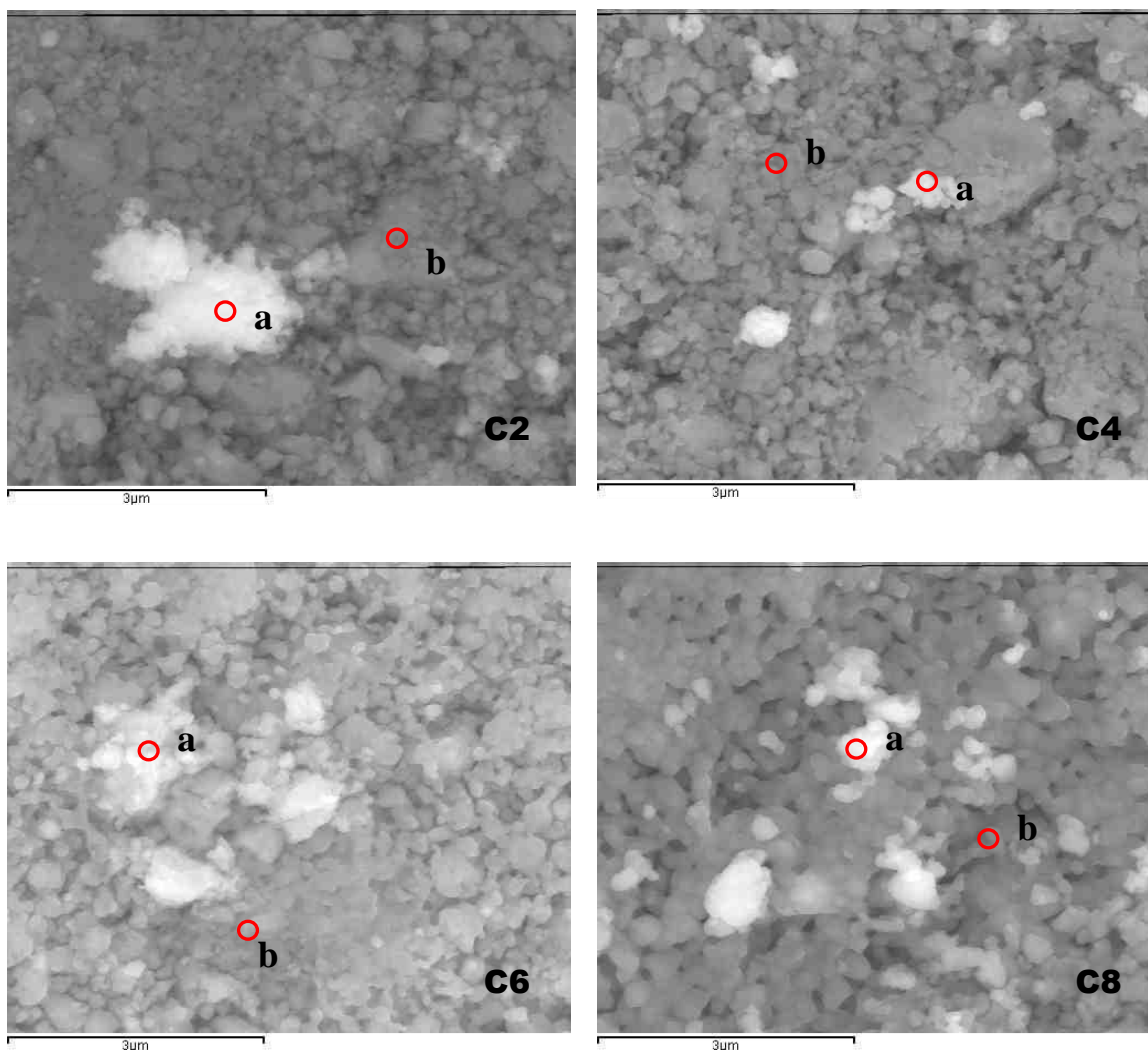


**Figure 3.** SEM images of  $\text{Li}_{1+x}\text{Cr}_x\text{Sn}_{2-x}\text{P}_3\text{O}_{12}$  samples

### 3.3. Energy Dispersive X-ray Spectroscopy (EDX)

EDX analysis was done at different points (a and b indicated in Fig. 3) to confirm stoichiometric proportions of the samples and the EDX backscattered spectra are shown in Fig. 4. Table 1 lists the atomic percentage at both points a and b in Fig. 3. Since  $\text{Li}^+$  ion was not detectable by EDX, the concept of charge neutrality was employed [20-21]. Using this concept, it was found that the stoichiometries of the samples were in good agreement with the designated values. Thus EDX analysis indicated that  $\text{Cr}^{3+}$  was successfully substituted into  $\text{LiSn}_2\text{P}_3\text{O}_{12}$  matrix forming  $\text{Li}_{1+x}\text{Cr}_x\text{Sn}_{2-x}\text{P}_3\text{O}_{12}$  compounds.

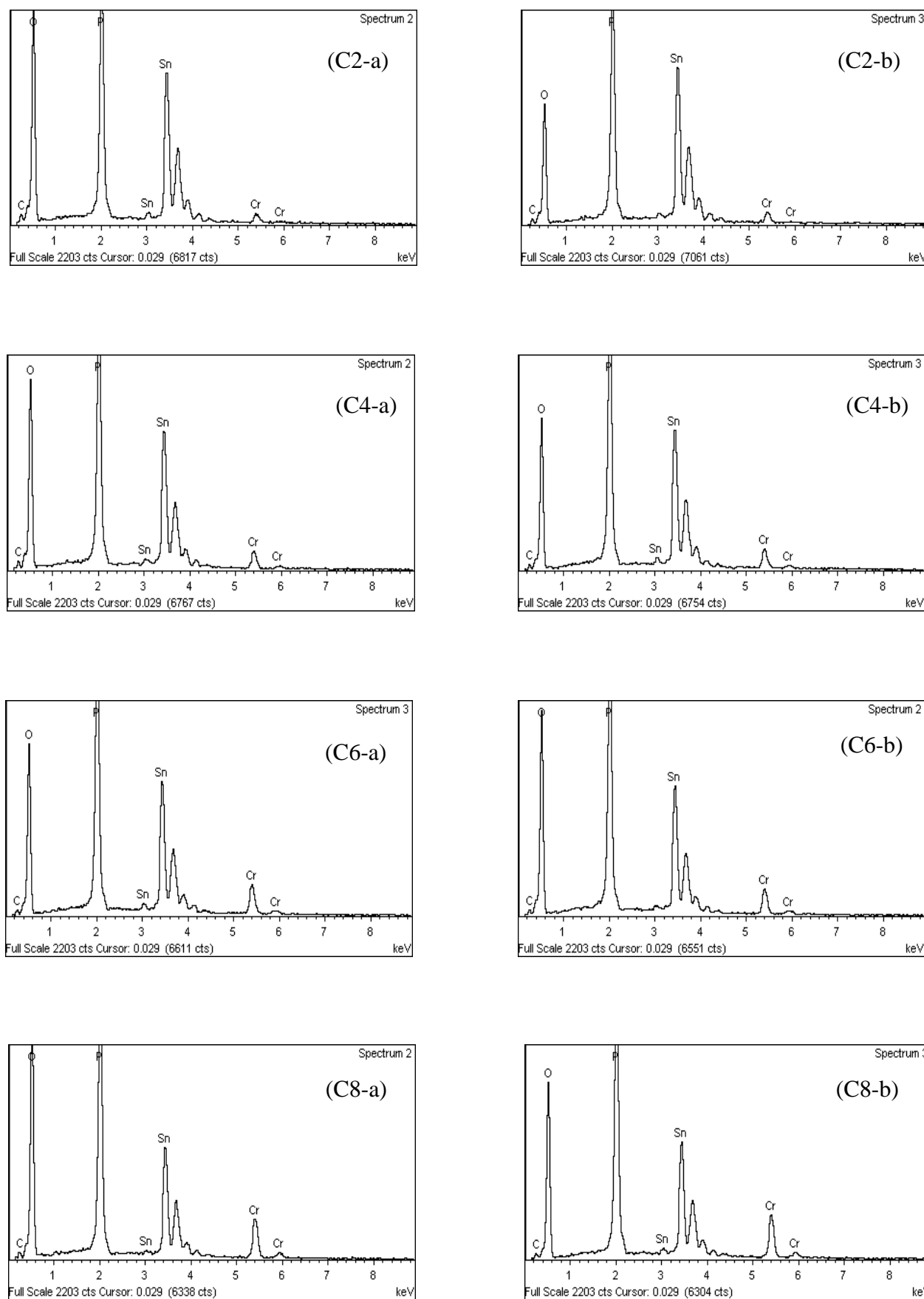


Figure 4. EDX spectra at both points a and b for all samples

**Table 1.** Atomic percentage of elements at points a and b for all samples

Sample	Composition		Elements (Atomic %)			Stoichiometric ratio Cr : Sn : P
			Cr	Sn	P	
C2	starting mixture		4	36	60	0.2 : 1.8 : 3.0
	EDX analysis	C2-a	3.56	35.54	60.90	0.17 : 1.75 : 3.00
		C2-b	4.15	36.35	59.50	0.21 : 1.83 : 3.00
C4	starting mixture		7.98	32.02	60.00	0.4 : 1.6 : 3.0
	EDX analysis	C4-a	7.26	32.20	60.54	0.36 : 1.60 : 3.00
		C4-b	7.55	32.17	60.28	0.38 : 1.60 : 3.00
C6	starting mixture		12.01	28.03	59.96	0.6 : 1.4 : 3.0
	EDX analysis	C6-a	11.46	28.26	60.28	0.57 : 1.41 : 3.00
		C6-b	11.94	27.92	60.14	0.60 : 1.39 : 3.00
C8	starting mixture		16.00	24.00	60.00	0.8 : 1.2 : 3.0
	EDX analysis	C8-a	15.45	23.66	60.89	0.76 : 1.17 : 3.00
		C8-b	15.86	23.71	60.43	0.79 : 1.18 : 3.00

3.4. Bulk Conductivity

Impedance plot ( $Z$  plot) for the sample with  $x = 0.2$  is presented in Fig. 5. The plot shows the presence of overlapping semicircles and an arc. The values of bulk resistance ( $R_b$ ) was determined from the intercept of the high frequency semicircle with the  $Z'$ -axis. The bulk ( $\sigma_b$ ) conductivity was calculated using the obtained  $R_b$  value and they are listed in Table 2. Since the semicircles in the impedance plot were quite difficult to be distinguished, confirmation of the obtained bulk conductivity was done by plotting the conductivity spectrum,  $\sigma$  plot (imaginary conductivity,  $\sigma''$  versus real conductivity,  $\sigma'$ ) of the sample. This method has been used by a few groups of researchers [22-26].

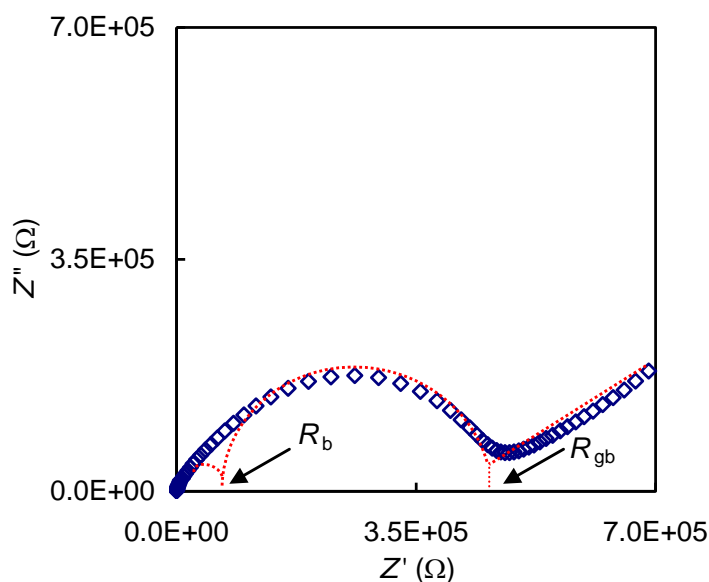


**Figure 5.** Impedance plot of C2

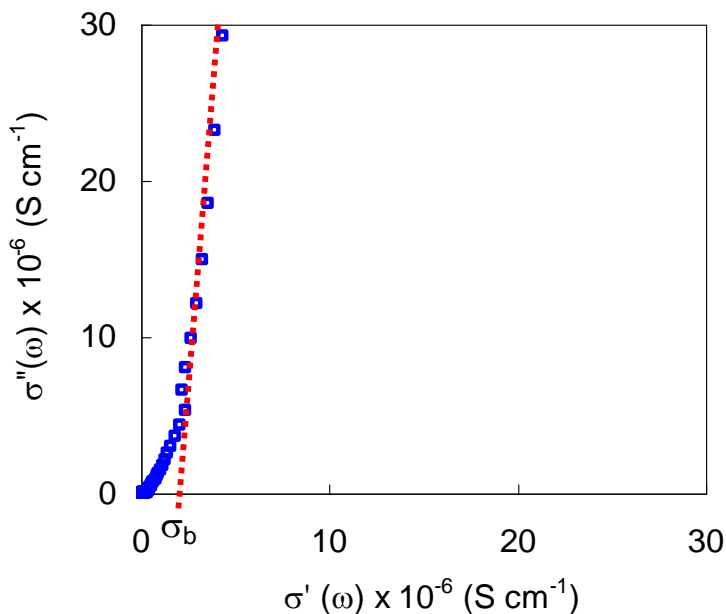


**Figure 6.** Conductivity plot of C2

The  $\sigma''$  versus  $\sigma'$  for C2 is depicted in Fig. 6. The figure shows the existence of two linear sections with different gradients (at high frequency region) and a semicircle (at low frequency region). Extrapolation of the first steeper section to  $\sigma'$  axis gave the value of bulk conductivity. Similar method was used to obtain conductivity for other samples.

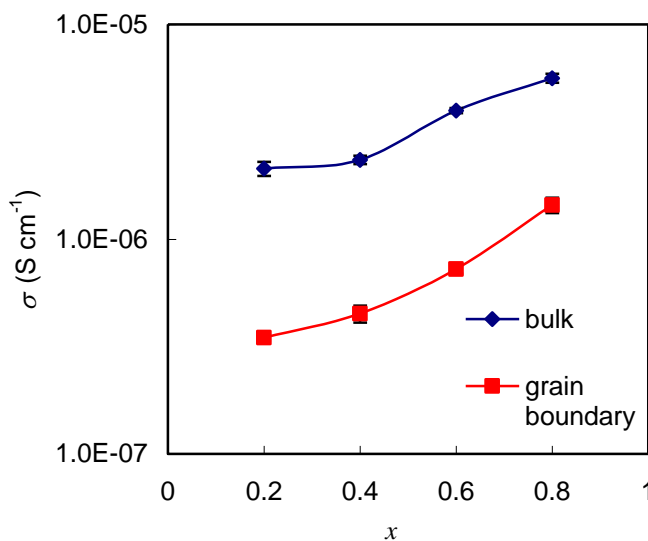


**Figure 7.** Variation of conductivity with x (chromium content)

It was observed that the values of bulk conductivity obtained from both impedance and conductivity spectra, Table 2, were marginally close to each other hence confirming the values of  $\sigma_b$  obtained from the impedance plots. Fig. 7 shows that both bulk and grain boundary conductivities

increased with increase in chromium content. The highest  $\sigma_b$  and grain boundary conductivity,  $\sigma_{gb}$  were observed for C8 with values of  $5.62 \times 10^{-6} \text{ S cm}^{-1}$  and  $1.44 \times 10^{-6} \text{ S cm}^{-1}$  respectively. This means that C8 showed an increase of three times of  $\sigma_b$  and about one order of magnitude of  $\sigma_{gb}$  of the unsubstituted  $\text{LiSn}_2\text{P}_3\text{O}_{12}$  which were  $1.65 \times 10^{-6}$  and  $1.05 \times 10^{-7} \text{ S cm}^{-1}$ , respectively [9].

The increase in conductivity with chromium content may be due to increase in the number of interstitial  $\text{Li}^+$  ions due to increase in the amount of  $\text{Cr}^{3+}$  ions [13]. Another factor that contributed to bulk conductivity enhancement was the increase in crystallinity which was the conducting structure in the compounds [13,19].

According to Semanate et al [20], the higher the structural order, the lower the energy barriers for ions to overcome in order to move. The enhancement in grain boundary conductivity was also attributable to improvement in contact between grains due to increase in homogeneity of grains as discussed in section 3.2. Semanate et al [20] also reported that similar grain sizes resulted in increase in the interfacial areas between grains. This increased the contact between grains which in turn increased conduction path and hence enhancing both bulk and grain boundary conductivities. Similar observations have reported by Best et al [2,27] and Mei et al [28].

The variations of conductivity with temperature for all samples are depicted in Fig. 8. For C2,  $\sigma_b$  showed two linear regions with different slopes with a sudden change in slope at 393 K. The linear regions showed that temperature dependent conductivity was thermally activated indicating Arrhenius behaviour [29-31]. The same trend was observed for other samples. However, the sudden change in slope was observed at 373 K. The bulk activation energy,  $E_{a,b}$  values are tabulated in Table 2. All samples showed similar  $E_{a,b}$  values at low temperature (low T) and high temperature (high T) regions. However the  $E_{a,b}$  in high T was lower than low T suggesting that there were two different diffusion channel [20,31].

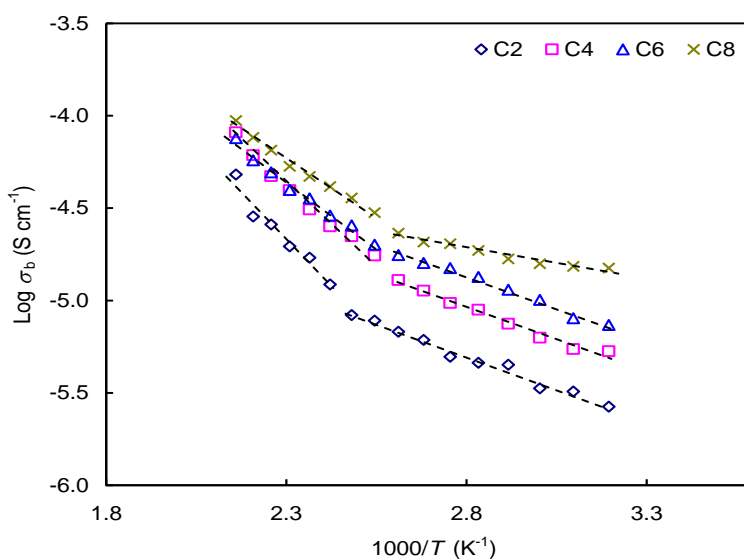


**Figure 8.** Temperature dependence of conductivity for  $\text{Li}_{1+x}\text{Cr}_x\text{Sn}_{2-x}\text{P}_3\text{O}_{12}$  samples

This was associated with a structure transition phenomenon from triclinic to rhombohedral structure [32]. Such structural transition occurred due to redistribution of  $\text{Li}^+$  ions. Losilla and co-workers [4] described that low temperature triclinic structure had low symmetry with ordered  $\text{Li}^+$  ions distribution. The structure had several bottleneck positions with a narrow probability for the  $\text{Li}^+$  ions to conduct. As temperature increased,  $\text{Li}^+$  bonds became loose making it free to move and became randomly distributed. At the same time, the torsion on  $\text{PO}_4$  tetrahedra takes place due to the frameworks accommodating themselves without breaking their bonds [17]. As a result  $\text{PO}_4$  tetrahedra rotated around two fold symmetry while  $\text{SnO}_6$  octahedra rotated in the opposite direction to its direction of rotation at low temperature forming restructured frameworks [33]. These restructured frameworks possessed a more appropriate bottleneck arrangement for the hopping of  $\text{Li}^+$  ions to take place. According to Kolher and Schulz [34], with increasing temperature, the bottleneck size increased hence ideally for diffusion of  $\text{Li}^+$  ion. As such, the probability of the  $\text{Li}^+$  ions to move increased causing redistribution of  $\text{Li}^+$  ions into lattice sites. This redistribution of lithium ions gave rise to a formation of a new structure (rhombohedral) which was a more conducting structure.

**Table 2.** Comparison of bulk conductivity values of  $\text{Li}_{1+x}\text{Cr}_x\text{Sn}_{2-x}\text{P}_3\text{O}_{12}$  samples obtained from impedance and conductivity plots together with activation energy and transference number values.

$x$	$\sigma_b \times 10^{-6} (\text{S cm}^{-1})$		$E_{a,b} (\pm 0.01) \text{ eV}$		$\tau_{\text{ion}}$
	Z plot	$\sigma$ plot	Low T	High T	
0.2	2.13 ( $\pm 0.03$ )	2.11 ( $\pm 0.01$ )	0.10	0.02	0.97
0.4	2.34 ( $\pm 0.02$ )	2.35 ( $\pm 0.04$ )	0.09	0.02	0.97
0.6	3.97 ( $\pm 0.02$ )	3.96 ( $\pm 0.03$ )	0.09	0.03	0.99
0.8	5.62 ( $\pm 0.02$ )	5.61 ( $\pm 0.01$ )	0.07	0.04	0.99

The values of  $E_{a,b}$  also indicated that mobility of ions was not varied. As such, the increase in conductivity may be due to increase in polarisability of Cr ions and possible disorder of occupancy of vacant sites. Similar observation has been reported by Chowdari et al [29]. While Sugantha and Varadaraju [30] reported that the larger the polarisability of cation-oxygen bond, the easier the transport of ions through the bottleneck. Therefore it can be summarised that increase in  $\text{Cr}^{3+}$  ions, increased the ion transportation which resulted in an increase in conductivity.

### 3.5. Transference Number Measurement

Fig. 9 shows a typical plot of normalized polarisation current versus time for  $\text{Li}_{1+x}\text{Cr}_x\text{Sn}_{2-x}\text{P}_3\text{O}_{12}$  system. The polarisation current for all samples saturated after about 50 s as tabulated in Table 2. All samples showed transference number value close to unity. This shows that the conductivity of the  $\text{Li}_{1+x}\text{Cr}_x\text{Sn}_{2-x}\text{P}_3\text{O}_{12}$  electrolytes was predominantly ionic and was expected to be that of  $\text{Li}^+$  ions.

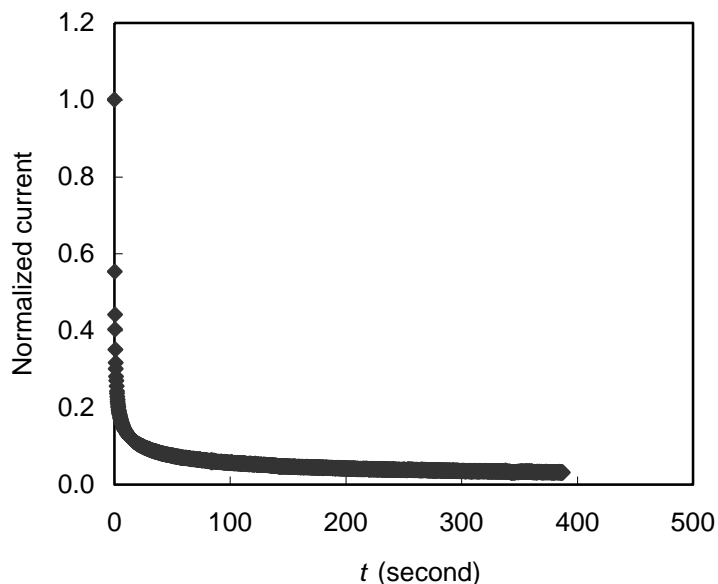


**Figure 9.** Typical plot of normalized polarisation current versus time for  $\text{Li}_{1+x}\text{Cr}_x\text{Sn}_{2-x}\text{P}_3\text{O}_{12}$  system

#### 4. CONCLUSIONS

Structural studies showed increase in crystallinity and homogeneity of the Cr substituted  $\text{LiSn}_2\text{P}_3\text{O}_{12}$  with increase in Cr content. EDX analysis indicated that Cr was successfully substituted at Sn sites in  $\text{LiSn}_2\text{P}_3\text{O}_{12}$  matrix. This was supported by the XRD results that showed changes in lattice constants as compared to the unsubstituted  $\text{LiSn}_2\text{P}_3\text{O}_{12}$ . SEM results showed increase in contact between grains due to grain with similar size when Cr is substituted into the parent compound. The substitution also resulted in conductivity enhancement up to to the order of  $10^{-6} \text{ S cm}^{-1}$ . Temperature dependent conductivity studies showed change in crystallography structure as reflected by different  $E_{a,b}$  values for high and low temperatures ranges. The enhancement in bulk conductivity with Cr content was attributed to increase in crystallinity and homogeneity of  $\text{LiSn}_2\text{P}_3\text{O}_{12}$  structure. Other factors of this enhancement were increase in number and polarisability of  $\text{Li}^+$  ions. The enhancement in both conductivities were also due to increase in  $\text{Li}^+$  migration as a result of increase in contact between grains.

#### References

1. J.Sanz, J.M. Rojo, R. Jimenez and J.E. Inglesias, *Solid State Ionics*, 62 (1993) 287.
2. A.S. Best, M. Forsyth and D.R. MacFarlane, *Solid State Ionics*, 136-137 (2000) 339.
3. K. Arbi, J.M. Rojo and J. Sanz. *Journal of The European Ceramic Society*, 27 (2007) 4215.
4. E.R. Losilla, M.A.G. Aranda, M.M. Lara and S. Bruque, *Chem. Mater.*, 9 (1997) 1678.
5. J.M. Winand, A. Rulmont and P. Tarte, *J. Solid State Chem.*, 93 (1991) 341.
6. A.M. Juarez, R. Jimenez. P.D. Martin, J. Ibanez and J.M. Rojo, *J. Phys. Condensed Matter*, 9 (1997) 4119.
7. M.G. Lazarraga, J. Ibañez, M. Tabellout and J.M. Rojo, *Compos. Sci. Technol.*, 64 (2004) 5759.

8. J. Angenault, J.C. Couturier, J.P. Souron, D. Siliqi and M. Quarton, *J. Mater. Sci. Lett.*, 11 (1992) 1705.
9. R. Norhaniza, R.H.Y. Subban and N.S. Mohamed, *Adv. Mater. Res.*, 129-131 (2010) 338.
10. X. Xu, Z. Wen, Z. Gu, X. Xu and Z. Lin, *Electrochem. Commun.*, 6 (2004) 1233.
11. C. Delmas, J.C. Viala, R. Olazcuaga, G.L. Flem and P. Hagemuller, *Mater. Res. Bull.*, 16 (1981) 83.
12. S.E. Sigaryov, *Mater. Sci. Engin.: B*, 13 (1992) 117.
13. X. Xu, Z. Wen, Z. Gu, X. Xu and Z. Lin, *Electrochem. Commun.*, 6 (2004) 1233.
14. W. Zhao, L. Chen and R. Xue, *Solid State Ionics*, 70/71 (1994) 144.
15. R. Norhaniza, R.H.Y. Subban and N.S. Mohamed, *J. Mater. Sci.*, 46 (2011) 24 7815.
16. J.E. Iglesias, J. Sanz, A.M. Juarez and J.M. Rojo, *J. Solid State Chem.*, 130 (1997) 322.
17. J. Alamo, *Solid State Ionics*, 63-65 (1993) 547.
18. F.J. Berry, N. Costantini and L.E. Smart, *Solid State Ionics*, 177 (2006) 2889.
19. C.J. Leo, B.V.R. Chowdari, G.V.S. Rao and J.L. Souquet, *Mater. Res. Bull.*, 37 (2002) 1419.
20. J.L.N. Semanate and A.C.M. Rodrigues, *Solid State Ionics*, 181 (2010) 1197.
21. F. Wu, Y. Liu, R. Chen, S. Chen and G. Wang, *J. Power Sources*. 189 (2009) 467.
22. A.F. Orliukas, A. Dindune, Z. Kanepe, J. Ronis, B. Bagdonas and A. Kezionis, *Electrochem. Acta*, 51 (2006) 6194.
23. R. Sobiestianskas, A. Dindune, Z. Kanepe, J. Ronis, A. Kezionis, E. Kazakevicius and A. Orliukas, *Mater. Sci. Engin. B*, 76 (2000) 184.
24. M. Cretin and P. Fabry, *J. European Ceramic Soc.*, 19 (1999) 2931.
25. M. Godickemeier, B. Michel, A. Orliukas, P. Bohac, K. Sasaki, L. Gauckler, H. Heinrich, P. Schwander, G. Kostorz, H. Hofmann and O. Frei, *J. Mater. Res.*, 9 (1994) 1228.
26. T. Šalkus, A. Kežionis, V. Kazlauskienė, J. Miškinis, A. Dindune, Z. Kanepe, J. Ronis, A.F. Orliukas, *Mater.Sci. Engin. B*, 172 (2010) 156.
27. A.S. Best, P.J. Newman, D.R. MacFarlane, K.M. Nairn, S. Wong and M. Forsyth, *Solid State Ionics*, 126 (1999) 191.
28. A. Mei, Q.H. Jiang, Y.H. Lin and C.W. Nan, *J. Alloys and Compounds*, 486 (2009) 871.
29. B.V.R. Chowdari, K. Radhakrishnan, K.A. Thomas and G.V.L Subba Rao, *Mater.Res. Bull.*, 24 (1989) 2221
30. M. Sugantha and U.V. Varadaraju, *Solid State Ionics*, 95 (1997) 201.
31. J.M.L Meins, O. Bohnke and G. Courbion, *Solid State Ionics*, 11 (1998) 67.
32. M.P. Screpel, F. d'Yvoire and E. Bretey, *Solid State Chemistry Proceedings of the Second European Conference*, (1982) 215.
33. J. Alamo and J.L. Rodrigo, *Solid State Ionics*, 63-65 (1993) 678
34. H. Kohler and H. Schulz, *Mater. Res. Bull.*, 20 (1985) 1461.